Ambiguities in Characterizing Stress States Involving Simple Shear

Journal of Physics: Conference Series **3104** (2025) 012048 doi:10.1088/1742-6596/3104/1/012048

Ambiguities in Characterizing Stress States Involving Simple Shear

Lilia Schuster[1], **Volker Schulze**[1], **Sebastian Münstermann**[2]

[1]Karlsruhe Institute of Technology (KIT), wbk Institute of Production Science, Kaiserstr. 12, 76131 Karlsruhe, Germany
[2]RWTH Aachen University, Institute of Metal Forming, Intzestr. 10, 52072 Aachen, Germany

E-mail: lilia.schuster@kit.edu

Abstract. For many applications, such as forming, crash, and cutting simulations, it is necessary to describe material behavior for large plastic strains or even until fracture occurs. For these types of finite element analysis, damage models are required to adequately describe changes in the stress-strain relationship. Many phenomenological damage models rely on the Lode parameter and stress triaxiality to characterize the stress state of a material element. However, these parameters alone are not sufficient to distinguish between coaxial and non-coaxial deformations. Non-coaxial deformations occur when the principal strain and principal stress axes do not remain aligned. The cause of this misalignment is the presence of simple shear during the deformation. This study utilizes Mohr's circle of strain to describe non-coaxial deformations and derives equations for various superpositions of biaxial stretch and simple shear. The equations to achieve specific Lode parameter and stress triaxiality pairs for variations of superposition are presented. Finite element simulations of single elements serve to validate these equations. These single-element simulations also demonstrate that, in non-coaxial deformations, the Lode parameter calculated from principal stress values differs from the Lode parameter calculated from principal strain values. The misalignment between principal stress and strain axes is a key to identifying simple shear. The findings of this study can contribute to improving damage models of ductile materials.

1 Introduction

Modeling material behavior up to the point of fracture requires complex material models. In particular, for metal sheets that exhibit elasto-plastic behavior and damage driven by microstructural changes, it is necessary to employ material models that consider the history of the material loading. The majority of phenomenological damage models in the current literature utilize the evolution of effective plastic strain depending on Lode parameter and stress triaxiality to describe the various stress states of the material. A fracture surface provides a value of failure strain for each Lode parameter/ stress triaxiality pair to account for the stress state dependency of the metal [1–8]. However, these parameters do not consider non-coaxial deformations. Consequently, this can lead to ambiguous stress state characterizations. The most prominent example is a stress state described by $L = 0, \eta = 0$. This is commonly referred to as simple shear. However, this deformation can also be achieved through pure shear deformation (Figure 1).

A pure shear deformation is equivalent to a deformation in plane strain condition without volume change. Simple shear is a deformation in which two sides of a cube slide parallel to each other and create the shape of a parallelepiped. Simple shear is always non-coaxial and is a special case of pure shear. A

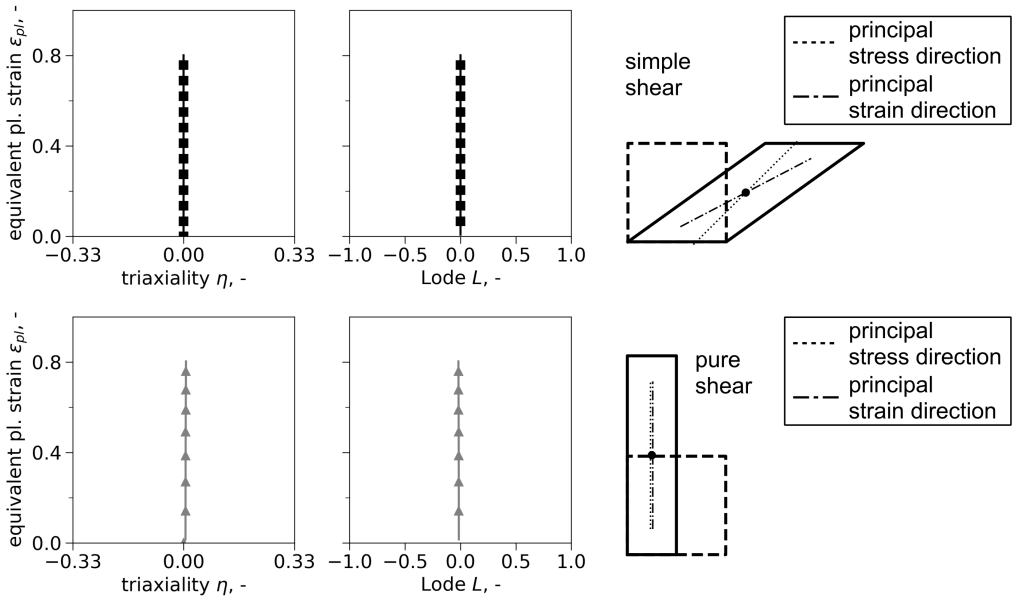

Figure 1: Equal strain paths for simple shear deformation (non-coaxial) and a pure shear deformation (coaxial) under plane strain condition

proportional loading with $L = 0, \eta = 0$ is not always a simple shear deformation, it can also be a pure shear deformation, which can be either non-coaxial or coaxial.

Butcher et al. demonstrated that mixing non-coaxial and coaxial characterization test in the process of determining model parameters for damage models can lead to different results [9]. Distinct microstructural evolutions during simple shear loading have been reported in previous studies [10].

In recent years, the topic of simple shear has gained increasing attention from researchers. A comprehensive and systematic overview of literature addressing simple shear in the field of metal material characterization was conducted by Han et al. in [11]. This extensive literature review covers the theoretical fundamentals, experimental technologies, mechanical responses, and structure-property relationships in regards to simple shear. They pointed out that the lack of a unified understanding and standardization has hindered the development of adequate simple shear testing methods, frameworks for consistent strain evaluation and development of appropriate constitutive models.

It is also worth examining studies in the field of geomechanics, where the topic of simple shear is also of interest. The need to distinguish non-coaxial deformations arising from simple shear from coaxial deformations has long been recognized in this field [12–14].

This study is a continuation of the work presented in [15], in which we focused on the superposition of uniaxial stretch with simple shear in plane stress. We demonstrated that the principal stress direction α_σ remains constant if the stretch perpendicular or parallel to the shear direction increases proportionally with the shear opening with a ratio of f_r, which describes the stretch/shear elongation ratio. The study also presented equations to calculate the Lode parameter L from f_r for non-coaxial deformations realized through superpositions of uniaxial stretch and simple shear. In addition, we presented the necessary steps to identify the amount of simple shear by reconstructing the deformation gradient.

The current study extends the work in [15] for superpositions of biaxial stretch with simple shear in plane stress. We can now show that for a fixed value of principal stress direction α_σ, and constant values of stretch/shear elongation ratio in x-direction f_{xx} and stretch/shear elongation ratio in y-direction f_{yy} the Lode parameter will change as the deformation progresses if neither f_{xx} nor f_{yy} is zero. We also present the equations for the Lode parameter L at the start of deformation for a superposition of biaxial stretch with simple shear. The principal stress direction α_σ, which remains constant during such a deformation can be calculated from f_{xx} and f_{yy}. These equations are also presented in this study.

2 Materials & Methods

2.1 Stress state in plane stress

The evolution of damage is driven by equivalent plastic strain, but it depends on the stress state of the material. Therefore, damage models describe the evolution of damage in relation to stress state parameters. Most commonly these parameters are stress triaxiality, Lode parameter and equivalent plastic strain. These stress state parameters can be expressed as functions of the principal stress components σ_1, σ_2 and σ_3, where σ_1 is the major principal stress, σ_2 is the intermediate principal stress, and σ_3 is the minor principal stress. The Lode parameter, Eq. (3), was originally proposed by Lode [16], and the stress triaxiality parameter, Eq. (2), was introduced by Bridgman [17]. We use σ_{vM} to abbreviate the von Mises equivalent stress Eq. (1).

$$\sigma_{vM} = \sqrt{\frac{1}{2}\left[(\sigma_1 - \sigma_2)^2 + (\sigma_2 - \sigma_3)^2 + (\sigma_3 - \sigma_1)^2\right]} \tag{1}$$

$$\eta_\sigma = \frac{\frac{1}{3}\left(\sigma_1 + \sigma_2 + \sigma_3\right)}{\sigma_{vM}} \tag{2}$$

$$L_\sigma = \frac{2\sigma_2 - \sigma_1 - \sigma_3}{\sigma_1 - \sigma_3} \tag{3}$$

For plane stress, the stress triaxiality η_σ and Lode parameter L_σ are uniquely related according to the following equation derived by Lou et al. in [18].

$$\frac{\sigma_1 + \sigma_3}{2} = \left(\eta_\sigma - \frac{L_\sigma}{3\sqrt{L_\sigma^2 + 3}}\right) \cdot \sigma_{vM} \tag{4}$$

We have added the subscript σ to indicate that stress values were used for the calculation of parameters L_σ and η_σ. The Lode parameter calculated from the principal stresses is not interchangeable with the Lode parameter calculated from principal strains for non-coaxial deformations.

To describe the Lode parameter from principal strain values instead of principal stress values, a relationship between the principal strain increments and the Lode parameter was derived by Lou et al. in [19]. This relationship helps to visualize the nature of stress states involving simple shear deformations, because the stress state parameters calculated from principal stresses differ from the analogous parameters calculated from the principal strains.

$$L_\varepsilon = \frac{3d\varepsilon_2}{d\varepsilon_1 - d\varepsilon_3} \tag{5}$$

$$\eta_\varepsilon\left(L_\varepsilon\right) = \begin{cases} -\frac{3-L_\varepsilon}{3\sqrt{L_\varepsilon^2+3}}, & \text{if } \sigma_1 = 0 \\ -\frac{2L_\varepsilon}{3\sqrt{L_\varepsilon^2+3}}, & \text{if } \sigma_2 = 0 \\ \frac{3+L_\varepsilon}{3\sqrt{L_\varepsilon^2+3}}, & \text{if } \sigma_3 = 0 \end{cases} \tag{6}$$

This study is limited to incompressible material, which is an appropriate assumption for metallic materials. Incompressibility can be described by a constant volume, which can be expressed by Eq. (7).

$$\begin{aligned} \left(1 + \varepsilon_{1,eng}\right)\left(1 + \varepsilon_{2,eng}\right)\left(1 + \varepsilon_{3,eng}\right) &= 1 \\ \varepsilon_{1,true} + \varepsilon_{2,true} + \varepsilon_{3,true} &= 0 \end{aligned} \tag{7}$$

The engineering strain ε_{eng} is simply the ratio between current length and original length of a deformation. Engineering strain values ε_{eng} and true strain values ε_{true} can be related by $\varepsilon_{true} = log(1 + \varepsilon_{eng})$. Here *log* refers to the natural logarithm. Additionally, the findings of this study assume a von Mises material.

Since the elastic part of the total strain is negligible, we will be using ε_{eff} according to Eq. (8) in some plots.

$$\varepsilon_{\text{eff}} = \sqrt{\frac{2}{3}\left(\varepsilon_{1,true}^2 + \varepsilon_{2,true}^2 + \varepsilon_{3,true}^2\right)} \tag{8}$$

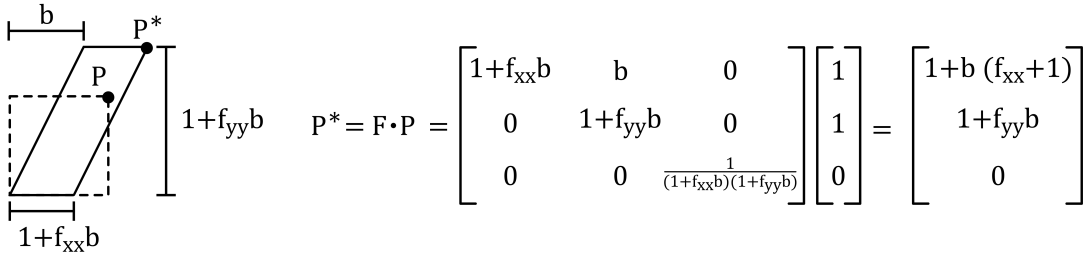

Figure 2: Deformation gradient F applied to a unit cube

2.2 Deformation gradient

Eq. (9) shows an example of a deformation gradient F that describes a superposition of simple shear with biaxial stretch. For simple shear superimposed with uniaxial stretch, either f_{xx} or f_{yy} is set to zero. The values f_{xx} and f_{yy} can have negative or positive values. We will call these parameters the stretch/shear elongation ratios in x-direction and y-direction respectively. The amount of shear opening is determined by the value of b. It is important to note that uniaxial stretch in our study refers to a uniaxial stretch in the plane of non-zero stresses. The length in z-direction also changes to preserve the volume. The same applies to the term biaxial stretch in this context.

The deformation gradient is used to translate a point in space P to a new point in space after deformation P^*. Figure 2 shows an example of the deformation of a unit cube into a new deformed state, which is comprised of a superposition of biaxial stretch and simple shear. The entries on the diagonal describe the lengths in x,y and z-direction after deformation. As we have set the volume of the cube to be constant, the entry in z-direction is the reciprocal of the product of F_{11} and F_{22} and is a direct result of Eq. (7). Because the original edge length of the cube is one unit, the entries are equal to the engineering strain. The entry in F_{12} is the result of simple shear.

To calculate the new position of point $P = [1, 1, 0]$ after applying the deformation described by F in Eq. (9), we calculate the product of F and P. The resulting vector P^* is the new position of P. This transformation can be repeated for each corner of the cube to calculate its new position. For a three-dimensional problem the deformation gradient is a 3 x 3 tensor. When simple shear is involved, the tensor is non-symmetric. This is the advantage over using the Cauchy strain tensor, which is symmetric and, therefore, does not consider simple shear.

The rate of deformation is another way to describe the progression of deformation. The description of superpositions of biaxial stretch with simple shear using the rate deformation tensor was described in [14]. The author also considered rigid body rotation during deformation. The method has been used in the context of geomechanics. The implications on phenomenological damage calculations were not discussed and effects on the calculation of stress state descriptors such as Lode parameter and stress triaxiality were not part of the study.

$$F = \begin{bmatrix} F_{11} & F_{12} & F_{13} \\ F_{21} & F_{22} & F_{23} \\ F_{31} & F_{32} & F_{33} \end{bmatrix} = \begin{bmatrix} 1 + f_{xx}b & b & 0 \\ 0 & 1 + f_{yy}b & 0 \\ 0 & 0 & \frac{1}{(1+f_{xx}b)(1+f_{yy}b)} \end{bmatrix} \tag{9}$$

2.3 Mohr's circle of strain

Although Mohr's stress circle is a popular tool for describing the stress tensor in the field of metal characterization, its counterpart, Mohr's strain circle, is less frequently utilized. This might be due to the fact that for application of metal processes involving sheet metals, we often deal with plane stress conditions. The exact opposite is true in geomechanics, where the problems can often be described by plane strain condition which makes this 2D representation of strain a popular tool in this field. The advantage of Mohr's circle of strain over the Mohr's circle of stress is, that it can visualize simple shear. The offset of the center of Mohr's circle of strain in y-direction is a direct result of simple shear. Mohr's circle of strain is based on the deformation gradient and therefore takes into account the asymmetry of the tensor. Since we are using an incompressible material, we can make use of Mohr's circle of strain for our plane stress problem, even though it was originally designed for plane strain problems. Transforming Mohr's circle of strain into 3D space is more complicated. In [20] a 3D representation using cyclides was suggested.

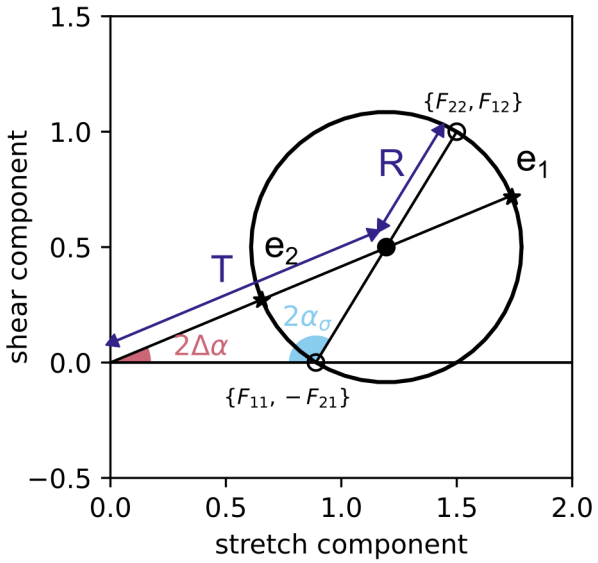

Figure 3: Mohr's circle of strain

Mohr's circle of strain is constructed by first marking the points $\{F_{11}, -F_{21}\}$ and $\{F_{22}, F_{12}\}$. The center of Mohr's circle is indicated at the halfway point between these two points. Then a circle is drawn through both points. The next step is to draw a line through the origin of the plot and the origin of the circle. This line will intersect the circle in two points. The distance between the origin and the further intersecting point on the circle is the magnitude of the major stretch value e_1, and the second intersecting point is the magnitude of a second stretch value e_2. This can be either the intermediate or the minor stretch value. Fig. 3 shows the values necessary for constructing Mohr's circle of strain. The figure also depicts the angle of principal stress direction α_σ and the angle offset between principal stress and principal strain direction $\Delta\alpha$. We will now use Mohr's circle of strain to calculate the Lode parameter at the beginning of a deformation.

First we calculate the distance between the origin of the plot and the center of the circle (T).

$$T = \frac{1}{2} \cdot \sqrt{(2 + b \cdot (f_{xx} + f_{yy}))^2 + b^2} \tag{10}$$

Then we calculate the radius of the circle (R).

$$R = \frac{b}{2} \cdot \sqrt{(f_{xx} - f_{yy})^2 + 1} \tag{11}$$

We do not know whether the second intersecting point on the circle represents the intermediate or minor stretch value. Therefore, we must distinguish between two cases. For the first case, the stretches can be calculated using

$$e_1 = T + R \tag{12}$$

$$e_2 = \frac{1}{T^2 - R^2} \tag{13}$$

$$e_3 = T - R \tag{14}$$

For the second case e_1 is the same as in (12), but the equations for e_2 and e_3 are interchanged.

Instead of using incremental values in Eq. (5), we will use absolute values, because we only want to calculate the Lode parameter L_σ at the start of the deformation. We insert the values for the stretches into Eq. (5). The stretches are applied to a unit cube with edge length 1. This means that the stretches in Eqs. (12)-(14) are equal to the engineering strains. These can be converted to true strains by applying the natural logarithm. Depending on whether Eq. (13) is greater or less than (14), the following equations result for the Lode parameter depending on geometric values of Mohr's circle of strain.

$$L_\varepsilon(b) = \frac{3 \cdot \log\left(\frac{1}{T^2 - R^2}\right)}{\log\left(\frac{T+R}{T-R}\right)}, \qquad T - R \leq \frac{1}{T^2 - R^2} \tag{15}$$

$$L_\varepsilon(b) = \frac{3 \cdot \log(T-R)}{\log\left((T+R)^2(T-R)\right)}, \quad T-R \geq \frac{1}{T^2-R^2} \tag{16}$$

At the start of deformation L_σ is equal to L_ε. The value at the start of deformation is calculated by determining the limit with b approaching 0, that is $\lim_{b\to 0} L_\sigma(b)$. For case 1, we get

$$L_\sigma(b=0) = -\frac{3 \cdot (f_{xx}+f_{yy})}{\sqrt{1+(f_{xx}-f_{yy})^2}}, \quad \eta \leq \frac{1}{3} \tag{17}$$

For case 2 we get

$$L_\sigma(b=0) = \frac{3 \cdot (f_{xx}+f_{yy}) - 3 \cdot \sqrt{1+(f_{xx}-f_{yy})^2}}{3 \cdot (f_{xx}+f_{yy}) + \sqrt{1+(f_{xx}-f_{yy})^2}}, \quad \eta \geq \frac{1}{3} \tag{18}$$

The value is the same for L_σ and L_ε at the beginning of deformation, because the principal stress and principal strain direction coincide at the start. When the deformation progresses these values will diverge. This will be discussed later in this study.

In [15] where these equations were derived for uniaxial stretch superimposed with simple shear, it was shown that the Lode parameter L_σ remains constant and is directly related to the direction of principal stress. This is no longer the case for biaxial stretch superimposed with simple shear.

Although Mohr's circle of strains is based on strain values, th value of the principal stress direction L_σ can be directly determined from this representation. It is half of the angle between the horizontal axis of the plot and the line connecting the construction points $\{F_{11}, -F_{21}\}$ and $\{F_{22}, F_{12}\}$. Note that the angle in the plot is twice as large as the actual angle of the principal stress direction. By using geometrical relationships, we can calculate the angle α_σ using Eq. (19).

$$\alpha_\sigma = \frac{\pi}{4} + \frac{1}{2} \cdot \arccos\left(\frac{1}{\sqrt{1+(f_{xx}-f_{yy})^2}}\right) \tag{19}$$

This equation is independent of b. This means that the angle of principal stress will remain constant as long as f_{xx} and f_{yy} remain constant during the deformation. We will validate this by using one-element tests.

2.4 Finite element simulation

Finite element simulations of one-element cubes were performed to validate the equations established in section 2.3. We used the Swift-Voce model to describe the stress-strain behavior of the von Mises material. As the name suggests, it is made up of two models,: the Swift-model with material parameters A, ε_0, n; and the Voce-model with material parameters k_0, Q, β_0. The parameter α controls the contribution of each part. Overall the Swift-Voce model uses seven parameters, Eq. (20). The Swift-Voce parameters for the simulations in this study are listed in Table 1. The resulting material corresponds to a DP600 steel sheet. The material model and parameter identification for the steel are described in [21].

$$\sigma_{S-V} = \alpha \cdot A(\varepsilon_0+\varepsilon_p)^n + (1-\alpha) \cdot (k_0 + Q(1-e^{-\beta_0 \varepsilon_p})) \tag{20}$$

Three one-element tests were simulated with Abaqus/Explicit solver. The first element describes a proportional uniaxial stress loading condition without simple shear, which is a deformation with coaxial stretch. The boundary conditions of this element are described in Fig. 4. The velocity v_x for uniaxial stress is calculated using $v_x = \frac{dx}{dt}$ and dx according to Eq. (21).

$$dx = \begin{cases} (1+dy)^{\frac{L_\sigma+3}{L_\sigma-3}} - 1 & , \ \eta \leq \frac{1}{3} \\ (1+dy)^{-\frac{L_\sigma+3}{L_\sigma-3}-1} - 1 & , \ \eta \geq \frac{1}{3} \end{cases} \tag{21}$$

The second element is a uniaxial stretch superimposed with simple shear. The value of f_{xx} is set to zero and f_{yy} is calculated using Eq. (17), while setting $L = -1$. The resulting value for f_{yy} is 0.354.

The third element is a biaxial stretch superimposed with simple shear. One of these values, f_{xx} or f_{yy} must be assigned arbitrarily. We selected a value of $f_{yy} = 0.5$. The second value is calculated again using Eq. (17), setting $L = -1$. The resulting value for f_{xx} is -0.110.

	Fixed DOFs	Fixed nodes	Moving nodes	Prescribed motion
coaxial stretch	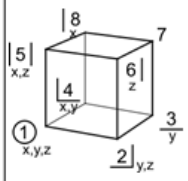	**x=0:** 1, 4, 5, 8 **y=0:** 1, 2, 3, 4 **z=0:** 1, 2, 5, 6	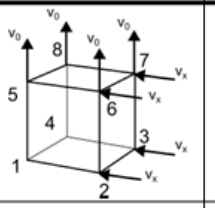	$\mathbf{v_0}$: 5,6,7,8 $\mathbf{v_x(t)}$: 2, 3, 6, 7
simple shear + **uniaxial** stretch	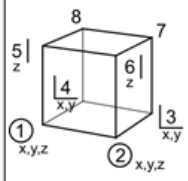	**x=0:** 1, 2, 3, 4 **y=0:** 1, 2, 3, 4 **z=0:** 1, 2, 5, 6	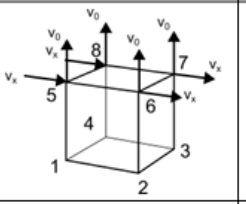	$\mathbf{v_0}$: 5,6,7,8 $\mathbf{v_x = f_{xx}\, v_0}$: 5,6,7,8
simple shear + **biaxial** stretch	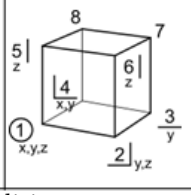	**x=0:** 1, 4 **y=0:** 1, 2, 3, 4 **z=0:** 1, 2, 5, 6	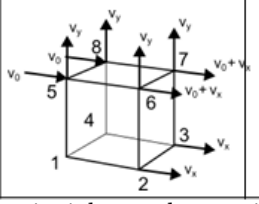	$\mathbf{v_0}$: 5, 8 $\mathbf{v_x = f_{xx}\, v_0}$: 2,3,6,7 $\mathbf{v_y = f_{yy}\, v_0}$: 5,6,7,8

Figure 4: Boundary conditions to create coaxial stretch, uniaxial stretch superimposed with simple shear and biaxial stretch superimposed with simple shear

Table 1: Swift-Voce parameters for DP600 [21]

Material	A	ε_0	n	k_0	Q	β_0	α
DP600	1045	0.001	0.36	797	418	43	0.64

3 Results & Discussion

In case of superposition of simple shear with uniaxial stretch either f_{xx} or f_{yy} is set to zero. The values for f_{xx} or f_{yy} can be inserted into the deformation gradient F according to Eq. (9) and used to plot Mohr's circle of strain.

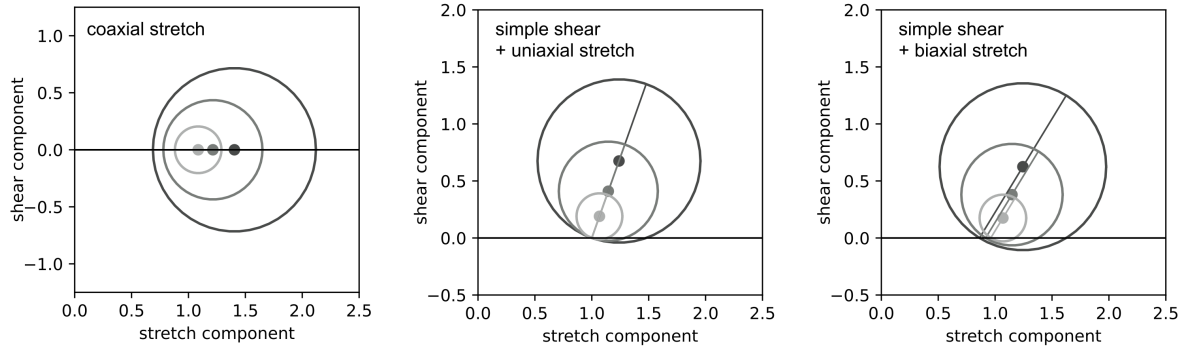

Figure 5: Evolution of Mohr's circle of strain for different deformation gradients applied to a unit cube

With increasing deformation, the radius of Mohr's circle of strain increases. Three circles are plotted to visualize different stages of the deformation (Fig. 5). The smallest circle is plotted at an effective strain value of $\varepsilon_{\text{eff}} = 0.25$, the middle circle is plotted at an effective strain of $\varepsilon_{\text{eff}} = 0.5$, the biggest circle is plotted at an effective strain of $\varepsilon_{\text{eff}} = 0.75$. ε_{eff} is the effective strain calculated from logarithmic strain values. The radius of each circle is directly linked to the effective strain value at the respective stage of deformation.

For a coaxial stretch deformation the center of the circle remains on the horizontal axis of the plot. This is because there is no skew value in the deformation gradient F (Eq. (9)) for coaxial stretch. For the

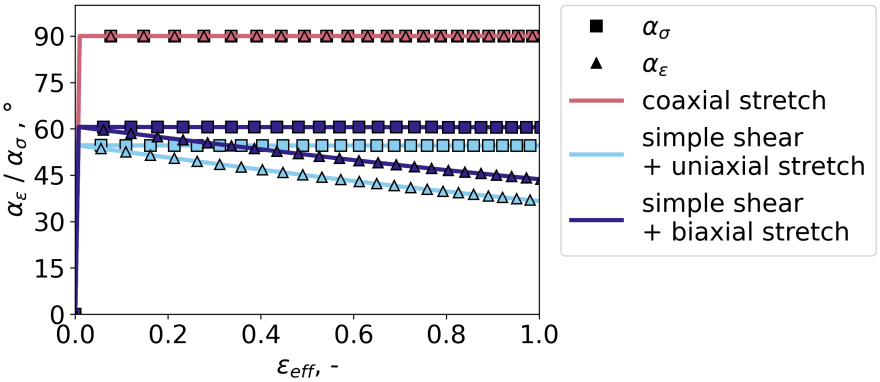

Figure 6: The evolution of angles of principal stress direction α_σ and principal strain direction α_ε

other two cases where simple shear is present, the center of the circle is not on the horizontal axis and travels upward as the non-coaxiality increases with progression of deformation. With the plot of uniaxial stretch superimposed with simple shear it is easy to see that the angle of principal stress α_σ remains constant. For the plot biaxial stretch superimposed with simple shear the angle is also constant. We now plot angle α_σ against the effective strain ε_{eff} to make this more evident (Fig. 6).

The theoretical value of the angle of principal stress direction can be calculated via equation (19) and is $\alpha_\sigma(f_{xx} = 0, f_{yy} = 0.354) = 54.74°$ for uniaxial stretch superimposed with simple shear with $f_{xx} = 0$ and $f_{yy} = 0.354$. For biaxial stretch superimposed with simple shear with $f_{xx} = -0.110$ and $f_{yy} = 0.5$, the theoretical value is $\alpha_\sigma(f_{xx} = -0.110, f_{yy} = 0.5) = 60.68°$. These angles remain constant during deformation. The results of the finite element simulation agree with the theoretical values. For coaxial stretch the angle is 90°. In this case the angle of principal stress direction α_σ and angle of principal strain direction α_ε are equal throughout the deformation, since it is a coaxial deformation. For the other two elements the angle of principal strain direction continue to diverge as the deformation progresses. This is evidence of the presence of simple shear and that this is indeed a non-coaxial deformation. We can imagine that by adjusting f_{xx} and f_{yy} during deformation, a constant strain path with constant values of L_σ and η_σ could be achieved. The resulting three strain paths calculated by principal stress values would then be indistinguishable. The description of a stress state using Lode parameter and stress triaxiality is therefore ambiguous.

The theoretical value for the Lode parameter at the beginning of the deformation is $L_\sigma = -1$ for all three deformations shown. By using both the Lode parameter L_σ calculated from principal stresses as well as Lode parameter L_ε calculated from principal strains we can visualize the non-coaxiality of the deformation. The Lode parameter L_σ calculated from principal stress remains constant for Fig. 7 and Fig. 8. If we were to only look at Lode parameter and stress triaxiality calculated from principal stresses we would assume that these two deformations traverse the exact same stress states. However, the deformation in (Fig. 7) is a coaxial deformation, the other deformation involving simple shear (Fig. 8) is non-coaxial. Therefore to adequately describe a stress state without ambiguity it might be necessary to introduce another stress state parameter. The results of this study can assist in developing experimental tests to compare deformations with and without simple shear traversing the same stain paths.

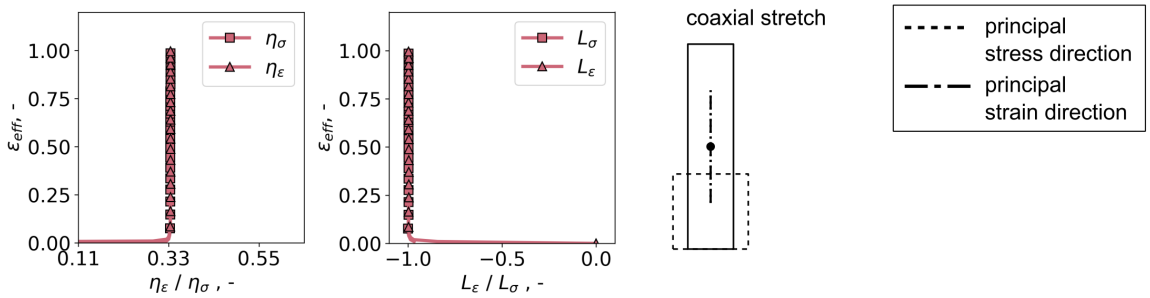

Figure 7: Strain paths calculated for coaxial stretch deformation with constant values of $L_\sigma, \eta_\sigma = (-1, \frac{1}{3})$

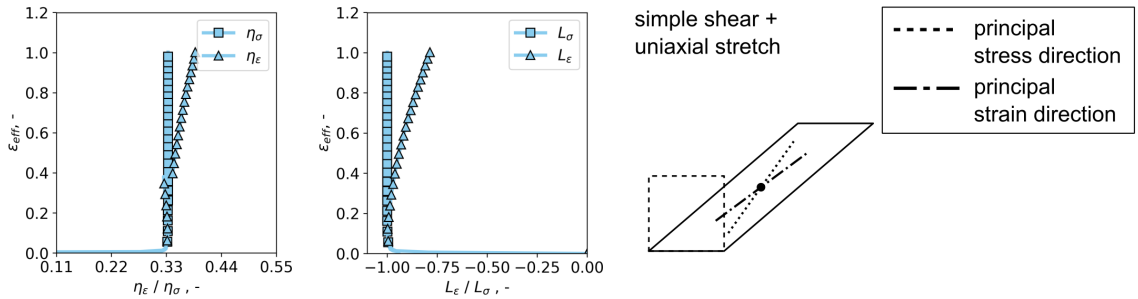

Figure 8: Strain paths calculated for uniaxial stretch superimposed with simple shear deformation with constant values of $L_\sigma, \eta_\sigma = (-1, \frac{1}{3})$

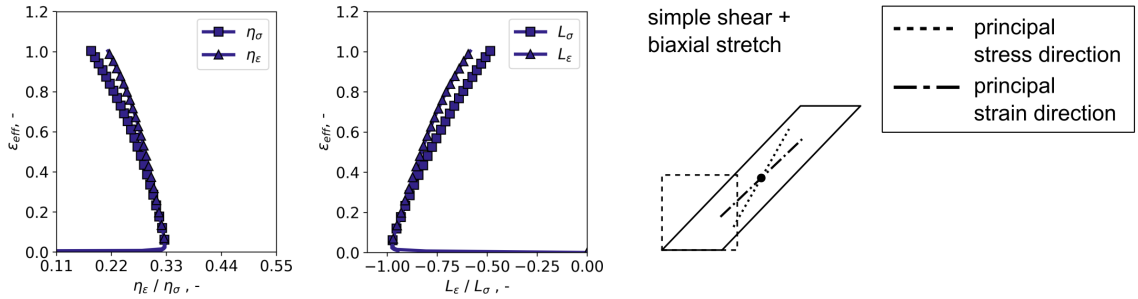

Figure 9: Strain paths calculated for biaxial stretch superimposed with simple shear deformation with starting value of $L_\sigma, \eta_\sigma = (-1, \frac{1}{3})$

4 Conclusion & Outlook

This study demonstrated that characterizing a stress state using Lode parameter and stress triaxiality leads to an ambiguous description. This method of describing stress states does not distinguish between coaxial and non-coaxial deformations.

Our study expanded on previous results where this ambiguity was discussed for cases of uniaxial stretch superimposed with simple shear. Additional equations considering biaxial stretch superimposed with simple shear were considered. While for uniaxial stretch superimposed with simple shear Lode parameter and stress triaxiality remained constant, if the principal direction of stress also remained constant, this is not the case for biaxial stretch superimposed with simple shear. A constant angle of the principal stress direction is not associated with a proportional strain path. It will be interesting to see how the stretch/shear elongation ratios for biaxial stretch need to change during deformation to achieve a proportional strain path.

It is a fact that coaxial and non-coaxial deformations occur during loading of sheet metals. This study provides a point of discussion on how to design characterization tests for different non-coaxial loading conditions and can assist in the development and improvement of damage models.

Acknowledgments

The authors received no financial support for the research, authorship, or publication of this article.

References

[1] Brünig M, Gerke S and Schmidt M 2018 *International Journal of Plasticity* **102** 70–82 ISSN 07496419 URL doi.org/10.1016/j.ijplas.2017.12.003

[2] Danas K and Ponte Castañeda P 2012 *International Journal of Solids and Structures* **49** 1325–1342 ISSN 00207683 URL doi.org/10.1016/j.ijsolstr.2012.02.006

[3] Cao T S, Gachet J M, Montmitonnet P and Bouchard P O 2014 *Engineering Fracture Mechanics* **124-125** 80–96 ISSN 00137944 URL doi.org/10.1016/j.engfracmech.2014.03.021

[4] Ganjiani M and Homayounfard M 2021 *International Journal of Solids and Structures* **225** 111066 ISSN 00207683 URL doi.org/10.1016/j.ijsolstr.2021.111066

[5] Xiao X, Mu Z, Pan H and Lou Y 2018 *International Journal of Impact Engineering* **120** 185–201 ISSN 0734743X URL doi.org/10.1016/j.ijimpeng.2018.06.008

[6] Chouksey M and Keralavarma S M 2022 *Journal of the Mechanics and Physics of Solids* **164** 104882 ISSN 00225096 URL doi.org/10.1016/j.jmps.2022.104882

[7] Erice B and Gálvez F 2014 *International Journal of Solids and Structures* **51** 93–110 ISSN 00207683 URL doi.org/10.1016/j.ijsolstr.2013.09.015

[8] Lian J, Sharaf M, Archie F and Muenstermann S 2013 *International Journal of Damage Mechanics* **22** 188–218 URL doi.org/10.1177/1056789512439319

[9] Butcher C and Abedini A 2019 *Metals* **9** 1052 ISSN 2075-4701 URL doi.org/10.3390/met9101052

[10] Renard K, Idrissi H, Schryvers D and Jacques P 2012 *Scripta Materialia* **66** 966–971 ISSN 13596462 URL doi.org/10.1016/j.scriptamat.2012.01.063

[11] Han G, He J, Li S and Lin Z 2024 *Progress in Materials Science* **143** 101266 ISSN 0079-6425 URL doi.org/10.1016/j.pmatsci.2024.101266

[12] Ramsay J G, Huber M I and Ramsay J G 2003 *Strain analysis* 7th ed (*The techniques of modern structural geology / John G. Ramsay; Martin I. Huber* no Vol. 1) (London: Academic Press) ISBN 978-0-12-576901-3 978-0-12-576921-1

[13] Passchier C 1988 *Tectonophysics* **149** 323–338 ISSN 00401951 URL doi.org/10.1016/0040-1951(88)90181-3

[14] Ramberg H 1975 *Tectonophysics* **28** 1–37 ISSN 00401951 URL doi.org/10.1016/0040-1951(75)90058-X

[15] Schuster L and Münstermann S **249** ISSN 1573-2673 URL https://doi.org/10.1007/s10704-025-00856-0

[16] Lode W 1926 *Zeitschrift für Physik* **36** 913–939 ISSN 1434-6001, 1434-601X URL doi.org/10.1007/BF01400222

[17] Bridgman P W 1964 *Studies in Large Plastic Flow and Fracture: With Special Emphasis on the Effects of Hydrostatic Pressure* (Harvard University Press) ISBN 978-0-674-73133-2 URL doi.org/10.4159/harvard.9780674731349

[18] Lou Y and Huh H 2013 *International Journal of Solids and Structures* **50** 447–455 ISSN 00207683 URL doi.org/10.1016/j.ijsolstr.2012.10.007

[19] Lou Y, Yoon J W and Huh H 2014 *International Journal of Plasticity* **54** 56–80 ISSN 0749-6419 URL doi.org/10.1016/j.ijplas.2013.08.006

[20] Coelho S and Passchier C 2008 *Journal of Structural Geology* **30** 580–601 ISSN 0191-8141 URL doi.org/10.1016/j.jsg.2008.01.003

[21] Schuster L, Olfert V, Sherepenko O, Fehrenbach C, Song S, Hein D, Meschut G, Biro E and Münstermann S 2024 *steel research international* **95** 2300530 ISSN 1869-344X URL doi.org/10.1002/srin.202300530